Small-Angle Neutron Scattering Analysis of Bottlebrush Backbone and Side Chain Flexibility

Stacy L. Pesek,[1,2] Qiqi Xiang,[1] Boualem Hammouda,[3] Rafael Verduzco[1,2,4]

[1]Department of Chemical and Biomolecular Engineering, Rice University, 6100 Main Street MS-362, Houston, Texas 77005
[2]Nanosystems Engineering Research Center for Nanotechnology-Enabled Water Treatment, Rice University, 6100 Main Street MS-362, Houston, Texas 77005
[3]National Institutes for of Standards and Technology, Center for Neutron Research, 100 Bureau Drive, Stop 6102, Gaithersburg, Maryland 20899-6102
[4]Department of Materials Science and NanoEngineering, Rice University, 6100 Main Street MS-325, Houston, Texas 77005
Correspondence to: R. Verduzco (E-mail: rafaelv@rice.edu)

Received 24 June 2016; accepted 22 September 2016; published online 4 October 2016
DOI: 10.1002/polb.24251

ABSTRACT: Bottlebrush polymers have densely tethered side chains grafted to a linear polymer backbone, resulting in stretching of both the side chains and backbone. Prior studies have reported that the side chains are only weakly stretched while the backbone is highly elongated. Here, scaling laws for the bottlebrush backbone and side chains are determined through small-angle neutron scattering analysis of a systematic series of poly(lactic acid) bottlebrush polymers synthesized via a "grafting-through" ring-opening polymerization. Scattering profiles are modeled with the empirical Guinier–Porod, rigid cylinder, and flexible cylinder models. Side chains are found to be only weakly stretched, with an end-to-end distance proportional to $N^{0.55}$, while the overall bottlebrush increases in size proportional to $N^{0.77}$. These results demonstrate that the bottlebrush backbone is not fully extended and that both side chains and backbone have significant conformational flexibility in solution. © 2016 Wiley Periodicals, Inc. J. Polym. Sci., Part B: Polym. Phys. **2017**, *55*, 104–111

KEYWORDS: bottlebrush polymers; poly(lactic acid); small-angle neutron scattering

INTRODUCTION Bottlebrush polymers represent a unique class of highly branched polymers, often with one or more grafted side chain per backbone repeating unit, resulting in steric repulsion between side chains and an extended cylindrical conformation. These types of polymers are of interest for a broad range of applications, from responsive surface coatings to nanoscale materials for drug delivery, as detailed in a number of recent reviews.[1–5] The conformation of bottlebrush polymers impacts their physical properties. For example, a sphere-to-globule transition with increasing backbone lengths is reflected in an extremely high entanglement molecular weight and weak dependence of the zero-shear viscosity of bottlebrush melts with molecular weight.[6] In another example, the length of the side chains has been shown to govern entropic de-wetting and segregation of bottlebrush polymers in blends.[7,8]

A number of studies have sought to understand the conformation of bottlebrush polymers and quantify the degree of stretching of both the backbone and side chains.[1] The conformation of the backbone and side chains can be described through analysis of the end-to-end distance as a function of the degree of polymerization (N). In general, studies have found that the side chains are only weakly stretched while the backbone is strongly elongated. Scaling theories predict that the side chain end-to-end distance scales with $N^{3/4}$ and $N^{2/3}$ in good and theta solvents, respectively, compared with $N^{3/5}$ and $N^{1/2}$ for free chains.[9–12] Simulations predict weaker stretching of the side chains in a good solvent, with an end-to-end distance that scales with $N^{1/2}$.[13]

Both experimental work and computational simulations have shown that the backbone is extended. Analysis of bottlebrushes adsorbed to a surface have reported a fully extended backbone (end-to-end distance scales with N),[14,15] while experiments on bottlebrush block copolymers have reported a domain spacing that scales approximately with $N^{0.9}$,[16–19] suggesting that bottlebrush backbones are not fully elongated and have some conformational flexibility.[16] Simulations have predicted an extended but more flexible backbone, with an end-to-end distance that scales with $N^{0.71}$ in a good solvent.[13]

Additional Supporting Information may be found in the online version of this article.

A number of studies have characterized the conformation of bottlebrushes in solution through scattering measurements,[20–29] but very few have analyzed a series of samples varying in backbone and side chain length. Furthermore, only a few investigations have studied bottlebrushes made using a "grafting-through" approach,[22–24] which guarantees full grafting density. We previously analyzed poly(norbornene)-*graft*-PS (PNB-*g*-PS) bottlebrushes through small-angle neutron scattering (SANS) measurements of dilute bottlebrush polymer solution.[22] Analysis of the scattering profile of dilute bottlebrush solutions provided the single molecular form factor, which revealed a shape transition from spherical to elongated bottlebrush polymers when the backbone degree of polymerization (DP) was sufficiently long (DP > 120).[22] This finding has been corroborated in subsequent scattering and rheological studies.[6,23] However, a limitation of our prior SANS study is that the series of bottlebrush polymers studied varied in both the length of the side chain and backbone, which made it difficult to quantify the conformation of the bottlebrush backbone and side chain separately.

Here, we seek to quantify the backbone and side chain conformation through quantitative analysis of a systematic, well-defined series of bottlebrushes in solution. We focus on a series of bottlebrush polymers with poly(lactic acid) (PLA) side chains. We characterize and analyze the series of bottlebrush polymers by SANS to extract a scaling relationship for the radius and length as a function of side chain and backbone DPs. Side chains are found to be only weakly stretched, with an end-to-end distance proportional to $N^{0.55}$ while the overall bottlebrush increases in size proportional to $N^{0.77}$. These results demonstrate that the bottlebrush backbone is not fully extended and that both side chains and backbone have significant conformational flexibility in solution.

EXPERIMENTAL

Materials

Lactide, stannous octoate, and solvents were purchased from commercial suppliers. Lactide was recrystallized from ethyl acetate twice prior to use. Anhydrous dichloromethane (DCM) was degassed with nitrogen prior to use. Modified Grubbs' catalyst ($(H_2IMes)(pyr)_2(Cl)_2RuCHPh$)[30] and N-(hydroxypentanyl)-*cis*-5-norbornene-*exo*-2,3-dicarboximide[31] were synthesized as previously described. The identification of commercial products does not imply endorsement by the National Institute of Standards and Technology nor does it imply that these are the best for the purpose.

Synthesis of Norbornene-Poly(D,L-Lactic Acid) (NB-PLA)

NB-PLA was synthesized via ring opening polymerization in a procedure modified from a previous study.[32] In a representative reaction, lactide (16.8 mmol, 2.42 g), *N*-(hydroxypentanyl)-*cis*-5-norbornene-*exo*-2,3-dicarboximide (0.67 mmol, 167.3 mg), and stannous octoate (0.013 mmol, 5.45 mg) were mixed and heated to 120 °C for 4 hours. The polymer was collected by precipitation in methanol to yield NB-PLA-57($M_n = 4361$ g mol^{-1}, $Đ = 1.29$). NB-PLA-37: ($M_n = 2678$ g mol^{-1}, $D = 1.41$).

Synthesis of Poly(Norbornene)-Graft-Poly(Lactic Acid) Bottlebrush Polymers (PNB-g-PLA)

Ring-opening metathesis polymerization (ROMP) of the NB-PLA macromonomers afforded bottlebrush polymers with polynorbornene backbones and PLA side chains. In a procedure modified from our previous report,[22] macromonomer NB-PLA-57 (0.101 g, 0.023 mmol) was added to a 5 mL round bottom flask equipped with a stir bar. The flask was vacuum dried and backfilled with nitrogen three times, followed by the addition of degassed DCM (0.05 mol L^{-1}). A stock solution of modified Grubbs' catalyst (0.01 g in 1.0 mL DCM) was added to the macromonomer solution at specified molar ratios. After 2 hours, the reaction was quenched by the addition of butyl vinyl ether (0.1 mL) followed by precipitation in 100 mL cold methanol. GPC analysis for all samples is provided in Figure S1.

Instrumentation

Gel-Permeation Chromatography (GPC)

Polymer molecular weights and molecular weight dispersities $Đ$ were obtained using an Agilent 1200 module equipped with three PSS SDV columns in series (100, 1000, and 10,000 Å pore sizes), an Agilent variable-wavelength UV/vis detector, a Wyatt technology HELEOS II multiangle laser light scattering (MALLS) detector ($\lambda = 658$ nm), and a Wyatt Technology OptilabreX RI detector. THF was used as the mobile phase at a flow rate of 1 mL min^{-1} at 40 °C. For bottlebrush polymer synthesis, macromonomer conversion was determined by comparing the integrated areas corresponding to bottlebrush polymer and unreacted macromonomer. Bottlebrush polymer dn/dc values were calculated by assuming 100% mass recovery.

Nuclear Magnetic Resonance Spectroscopy (NMR)

Proton NMR (^{1}H NMR) spectra were recorded using tetramethylsilane as an internal standard in $CDCl_3$ on a 400 MHz Bruker multinuclear spectrometer. Samples were placed in 5 mm o.d. tubes with a concentration of 10 mg mL^{-1}.

Small-Angle Neutron Scattering (SANS)

SANS measurements were performed at the National Institute of Standards and Technology Center for Neutron Research on the NG3 and NG7 30 m instruments with a neutron wavelength of $\lambda = 6$ Å. Three sample-detector distances were used (1.3, 4, and 15 m), providing an overall q range of 0.0014 Å$^{-1} < q < 0.4$ Å^{-1}. Polymer samples were prepared at a mass fraction of 1% in 1,4-dioxane-d_8 and allowed to equilibrate at RT for at least 4 hours before measurement. The series of samples was also analyzed in toluene-d_8, but they were found to aggregate strongly, precluding analysis to determine the single molecular form factor (see Figure S2). Temperature control was provided by a water circulation bath and was held constant at $T = 25$ °C. Scattering data were corrected for the solvent baseline with a scale factor (0.95–1.02) appropriate for the mass fraction of solvent. Model fitting was performed using NCNR Data Analysis IGOR

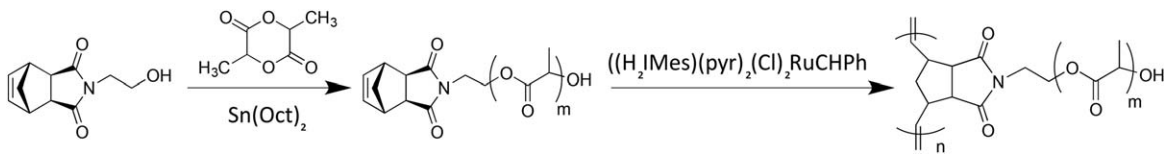

SCHEME 1 Synthesis of PNB-*g*-PLA bottlebrush polymers through ROMP of NB-PLA macromonomers.

PRO software[33] and the Guinier–Porod,[34] rigid cylinder,[35,36] and flexible cylinder[37] models. Model fitting was performed through nonlinear least squares and parameter uncertainty is determined through reduced chi-squared analysis to assign a confidence interval which represents one standard deviation of the Gaussian spread for each parameter.[38]

Transmission Electron Microscopy (TEM)

TEM was performed on JEOL 2010 TEM. Polymer solutions (0.1–1 mg mL^{-1} polymer in chloroform) were drop-cast onto carbon grids, dried, stained with 10% phosphotungstic acid (PTA), and immediately transferred to the microscope for imaging.

DISCUSSION

PNB-*g*-PLA bottlebrush polymers were prepared by ring-opening metathesis polymerization (ROMP) of norbornene terminated PLA macromonomers (see Scheme 1). Details on sample preparation, synthesis, and preliminary characterization are provided in the Supporting information. Due to extremely high reactivity and fast kinetics[32] of NB-PLA macromonomer, this chemistry allows for the synthesis of a well-defined series of bottlebrush polymers with systematically increasing backbone lengths (see Table 1). Side chain PLA macromonomers have molecular weights of approximately 2600 and 4300 g mol^{-1}, which corresponds approximately to side chain degrees of polymerization (N_{SC}) of 30 and 60, respectively. The precise molecular weights and N_{SC} values for all samples are reported in Table 1. PNB-*g*-PLA bottlebrushes with $N_{SC} \approx 30$ have molecular weights (M_w) 64.6–463 kg mol^{-1}, molecular weight dispersity $Đ$ less than 1.1, and macromonomer conversions greater than 90%. PNB-*g*-PLA bottlebrushes with $N_{SC} \approx 60$ have M_w 172–969 kg mol^{-1}, molecular weight dispersity $Đ$ less than 1.22, and macromonomer conversions greater than 95%. GPC analysis for all samples is provided in Figure S1.

Selected samples were analyzed by transmission electron microscopy (TEM), as shown in Figure 1. These measurements provided a size estimate for samples in the range of 15–28 nm for bottlebrushes tested (Table S1). While the bottlebrushes appear spherical, we note that this measurements are for dry bottlebrushes adsorbed to a substrate. We expect that adsorption to the substrate or solvent evaporation during casting can have an impact on polymer conformation and, therefore, provide only a rough estimate of bottlebrush size in solution.

We carried out small-angle neutron scattering (SANS) to quantify the conformation of the bottlebrushes as a function of side chain and backbone degrees of polymerization, N_{SC} and N_{BB}, respectively. SANS experiments were performed by dissolving PNB-*g*-PLA bottlebrushes at 1 wt% in 1,4-dioxane-d_8. The series of samples was also analyzed in toluene-d_8, but they were found to aggregate strongly, precluding analysis to determine the single molecular form factor in this solvent (see Figure S3 for corresponding scattering traces).

SANS data for PLA bottlebrushes in dioxane-d_8 are shown in Figure 2. The SANS traces can be qualitatively interpreted by focusing on three key regions.[22] Scattering at low-*q*

TABLE 1 Characteristics of NB-*g*-PLA Bottlebrushes Analyzed by Small-Angle Neutron Scattering

Bottlebrush (PLA N_{SC}–N_{BB})	$M_{n,SC}$[a] (g mol^{-1})	N_{SC}	[MM]/cat.	$M_{w,BB}$[b] (g mol^{-1})	$Đ$[b] (M_w/M_n)	N_{BB}[c]	% MM Conv[d]	*dn*/*dc*
PLA30–25	2630	34	25	64,600	1.06	25	90	0.051
PLA30–50	2680	34	50	138,000	1.10	52	98	0.056
PLA30–90	2680	34	100	234,000	1.09	87	99	0.052
PLA30–140	2680	34	150	386,000	1.11	144	100	0.051
PLA30–170	2680	34	200	463,000	1.11	173	99	0.050
PLA60–40	4550	60	50	172,000	1.22	38	95	0.049
PLA60–100	4360	57	100	421,000	1.11	97	99	0.045
PLA60–150	4360	57	150	643,000	1.13	147	99	0.046
PLA60–220	4360	57	200	969,000	1.14	222	99	0.042

[a] Determined from ^{1}H NMR end-group analysis.
[b] Absolute weight-averaged molecular weight and molecular weight dispersity of bottlebrush polymers calculated from GPC light-scattering analysis.
[c] Calculated using M_w for bottlebrush polymers and $M_{branch} \approx M_{n,SC}$ for PLA side chains.
[d] Conversion of NB-PLA calculated using GPC-RI analysis.

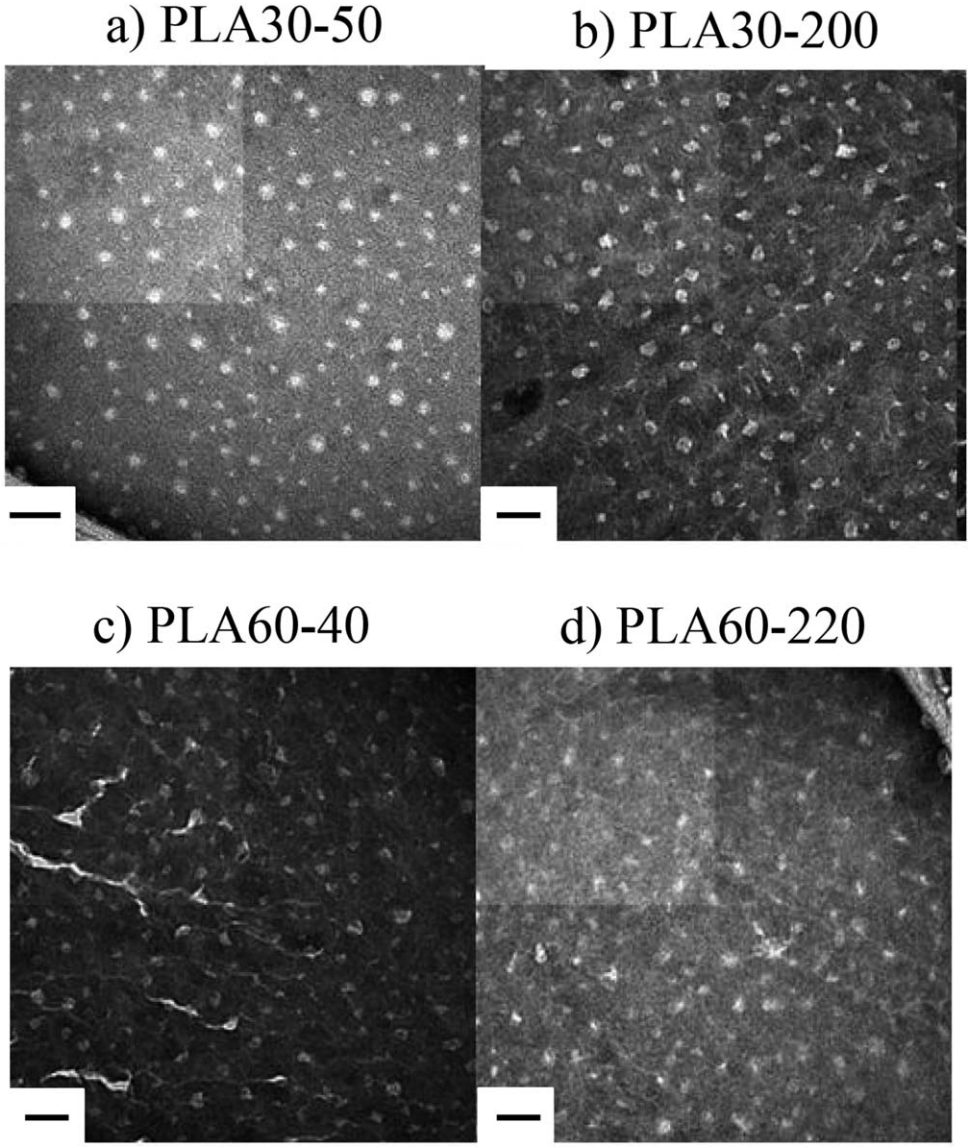

FIGURE 1 TEM micrographs of selected PNB-*g*-PLA bottlebrushes. (A) PLA30–50; (B) PLA30–200; (C) PLA60–40; and (D) PLA60–200. All scale bars are 50 nm.

($q < 0.03$ Å^{-1}) reflects the overall size and shape of the bottlebrush, and an upturn in the scattered intensity ($q < 0.01$ Å^{-1}) indicates some degree of intermolecular aggregation in solution. The middle-q region (0.03 Å$^{-1} < q < 0.1$ Å^{-1}) provides information about bottlebrush polymer length, shape, and cross-sectional area, and the high-q region ($q > 0.1$ Å^{-1}) reflects molecular-level thermal fluctuations. Within each series of PLA bottlebrushes with identical side chain lengths, the samples exhibit near quantitative overlap in the middle-q region, reflecting a constant cross-sectional area for bottlebrushes with similar side chain lengths. Bottlebrush polymers with longer backbones exhibit a pronounced upward slope in the q-range from 0.01 to 0.03 Å^{-1}, consistent with a more elongated molecular structure.

All samples exhibit some evidence for intermolecular aggregation, evidenced by a sharp upturn in scattering below $q = 0.01$ Å^{-1}. Clustering (observed as low-q upturn) has been reported both synthetic polymers and biomacromolecules in polar solvents.[39,40] Recent work has elucidated the potential sources of clustering in polar solvents, but the cause and structure of clusters is not fully understood.[39,41,42] We are unable to estimate a size for the aggregates since only an upturn in scattered intensity is observed. However, the features of the scattering curve corresponding to the molecular form factor are clearly separated from the upturn at low-q. In this work, we focus only on the region for which $q > 0.01$ Å^{-1} in order to extract the bottlebrush molecular form factor.

To quantitatively analyze the SANS data and extract single molecular details, we first apply the Guinier–Porod model, which is an empirical model applicable to objects of arbitrary shape.[34] This model is used as a starting point to understand general properties of the solution conformation

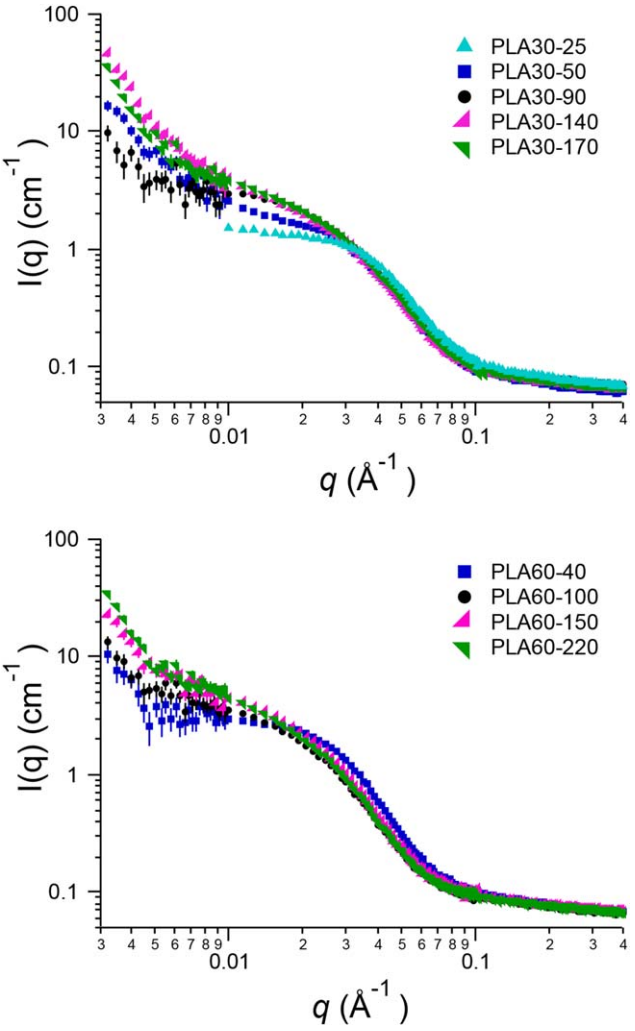

FIGURE 2 SANS traces for PNB-*g*-PLA bottlebrushes with N_{SC} = 30 (top) and N_{SC} = 60 (bottom) in 1,4-dioxane-d_8. Statistical uncertainties correspond to one standard deviation. [Color figure can be viewed at wileyonlinelibrary.com].

of the bottlebrushes. The Guinier–Porod model contains a total of three adjustable parameters: two parameters related to the molecular form factor (radius of gyration R_g and the dimension parameter s) and one (Porod factor P) related to scattering at high-q. The dimension parameter s reflects the anisotropy of the scattering particles, with 0 corresponding to a spherical globule and 1 a rod-like object. Intermediate values correspond to intermediate anisotropies. The Porod factor P sets the slope for $I(q)$ in the high-q region. More detailed discussion of this model is available in the published literature.[34,43] The model produces a reliable fit to the scattered intensity, as shown in Figures S3 and S4.

As shown in Table 2, the Guinier–Porod model predicts similar values of the radius of gyration R_g for bottlebrushes with the same side chain DP. For bottlebrushes with N_{SC} = 30, the Guinier–Porod model gives R_g, between 37.7 and 50.4 Å, while for N_{SC} = 60 the R_g is 53.4–60.4 Å. This is consistent with our prior study, where we concluded that R_g from the Guinier–Porod model reflects the bottlebrush radius.[22] As shown in Table 2, the dimension parameter s increases with N_{BB}, and thus the model of the scattered intensity indicates the bottlebrushes transition from spherical to rod-like globules with increasing N_{BB}. This was observed in our prior study with PS bottlebrushes[22] and has been observed others.[6,24] Although a completely empirical model, the Guinier–Porod model successfully captures the sphere-to-rod transition in the bottlebrush series with increasing backbone DP.

We next analyzed the scattering data using a rigid cylinder and flexible cylinder models. The rigid cylinder model contains two adjustable parameters, the radius R and bottlebrush length L, and assumes that the bottlebrush is a rigid cylinder.[35,36] The model adequately reproduces the scattered intensity in the mid- and low-q regions, as shown in Figures S65 and S6. We note that the model is not extended to the high-q region since this portion of the scattered intensity is not captured by a molecular form factor, but rather a power-law decay as in the Porod model. Parameter values along with uncertainties are presented in Table 2. The rigid cylinder model predicts a bottlebrush radius that is close to the R_g values predicted by the Guinier–Porod model but much more consistent across samples with similar side chain lengths, roughly 44.8 ± 2.0 Å for N_{SC} = 30 and 59.6 ± 3.1 Å for N_{SC} = 60. Error bars obtained from fitting correspond to one standard deviation. The cylinder length L increases with the backbone DP for both side chain series. Consistent with the predictions of the Guinier–Porod model, the rigid cylinder model indicates that as the backbone DP increases, the bottlebrush aspect ratio increases significantly. The bottlebrush radius remains constant, but the overall sample length increases rapidly with backbone DP.

Next, we analyzed the scattered intensity using the flexible cylinder model.[37] The flexible cylinder model contains three adjustable parameters: the contour length (CL), Kuhn step length (λ_K), and a radius (R). Using the values from the rigid rod model as a starting point along with an initial guess of

TABLE 2 Results from Best-Fit of Guinier–Porod Model to Scattered Intensity for PNB-*g*-PLA Bottlebrushed in 1,4-Dioxane-d_8

Polymer	S	R_g (Å)	P
PLA30–25	0.0	41.1 ± 0.07	3.5 ± 0.02
PLA30–50	0.05 ± 0.02	48.0 ± 0.47	3.0 ± 0.01
PLA30–90	0.31 ± 0.01	47.0 ± 0.37	3.1 ± 0.01
PLA30–140	0.67 ± 0.01	38.6 ± 0.40	3.0 ± 0.01
PLA30–170	0.72 ± 0.01	37.2 ± 0.60	3.1 ± 0.01
PLA60–40	0.0	59.8 ± 0.10	3.5 ± 0.01
PLA60–100	0.38 ± 0.02	60.4 ± 0.75	3.1 ± 0.01
PLA60–150	0.51 ± 0.02	56.6 ± 0.65	3.2 ± 0.01
PLA60–220	0.63 ± 0.02	53.4 ± 0.63	3.3 ± 0.01

Statistical uncertainties correspond to one standard deviation.

TABLE 3 Results from Best-Fit of Rigid and Flexible Cylinder Models to Scattered Intensity for PNB-*g*-PLA Bottlebrush Polymers in 1,4-Dioxane-d_8

	Cylinder		Flexible Cylinder		
Polymer	*L* (Å)	*R* (Å)	CL (Å)	*R* (Å)	λ_K (Å)
PLA30–25	78 ± 29.7	47.2 ± 8.1	81.2 ± 1	41.5 ± 0.1	142 ± 2
PLA30–50	150 ± 1.1	43.2 ± 0.2	149 ± 1	42.7 ± 0.3	187 ± 10
PLA30–90	213 ± 1.7	43.6 ± 0.1	227 ± 4	43.0 ± 0.3	160 ± 4
PLA30–140	241 ± 3.7	46.7 ± 0.2	319 ± 5	40.3 ± 0.2	169 ± 4
PLA30–170	297 ± 4.0	43.3 ± 0.2	386 ± 26	37.3 ± 1.3	105 ± 12
PLA60–40	156 ± 1.0	54.0 ± 0.2	151 ± 1	50.7 ± 0.1	257 ± 4
PLA60–100	264 ± 3.0	60.5 ± 0.2	451 ± 24	50.2 ± 0.6	112 ± 11
PLA60–150	306 ± 3.9	60.0 ± 0.2	462 ± 33	51.2 ± 1.0	116 ± 15
PLA60–220	425 ± 12.4	59.8 ± 0.2	482 ± 30	51.8 ± 0.3	126 ± 14

Statistical uncertainties correspond to one standard deviation.

168 Å for λ_K,[44] we were able to converge on best fit solutions with the flexible cylinder model for all samples in the series. The resulting parameter values are provided in Table 3, and a plot of the experimental data and model predictions are shown in Figures S7 and S8. In comparing the flexible cylinder model predictions to the rigid cylinder, the flexible cylinder predicts a modestly smaller *R*. The contour lengths are similar between the two models for backbone DPs less than 50, but for longer bottlebrushes the contour length CL is predicted to be much greater than the rigid rod length *L*. Plots comparing the model parameters predicted from the rigid cylinder and flexible cylinder model are shown in Figure S9.

The Kuhn lengths predicted from the flexible cylinder model fall in the range of 100–200 Å, consistent with prior scattering studies of bottlebrushes,[21,22,26,29,44] but no clear trend is observed in our model fitting results with either backbone or side chain lengths. While theoretical and computational studies uniformly predict that the persistence length of bottlebrush should increase with both side chain and backbone lengths,[10,11,13,20,45,46] experimental findings have been less clear. Several studies have measured a persistence length independent of backbone and side chain length for bottlebrush polymers,[21,22,24,47] while other experimental studies have found that the backbone of persistence length is a strong function of side chain length.[27,28,44,47–51] Our results are consistent with the former studies, but it is important to note that these various experimental studies report bottlebrush polymers that vary in a number of molecular parameters: side chain and backbone lengths, side chain composition, and grafting densities. For example, we would expect a very different rigidity and step-length for bottlebrushes based on a PNB backbone as in the present study compared with bottlebrushes based on a poly(methacrylate) backbone.[21] Furthermore, as Hsu et al.[13] note, simulations and scaling analysis predict a persistence length and rigidity for the bottlebrush backbone, while experiments measure rigidity for the entire bottlebrush polymer.

A comparison of the present set of materials to those studied previously by scattering can provide insight into the results of the model fit. For the particular samples under study, the overall bottlebrush length is roughly 2–3 times the expected Kuhn length and the ratio of the Kuhn length to the bottlebrush radius λ_K/R is 2–4. By comparison, in the studies by Rathgeber et al.[21] the backbone lengths exceeded 100 nm, and the ratio of the Kuhn length to the radius λ_K/R was roughly a factor of 10. Bolisetty et al.[26] reported bottlebrushes with very long backbones (DP of 1600 monomer units) and a ratio of λ_K/R exceeding 10. Similarly, in the studies by Zhang and Gröhn et al. studied bottlebrushes with backbone DPs exceeding 1000 and side chains of 30 units or less, and for their samples the ratio λ_K/R was larger than 10. Zhang et al.[24] studied bottlebrush polymers of a similar backbone and side chain size to those in the present study and found that both an ellipsoidal and a rigid cylinder model provided an accurate representation of the scattering data (results from a flexible chain model were not reported). In the present study, we note that the flexible chain model does provide an adequate fit for the scattered intensity, and the parameter values for the Kuhn lengths (10–20 nm) is comparable to what has been reported previously. However, the Kuhn length is found to decrease with increasing side chain length, and the flexible cylinder model predicts values with significant uncertainty, as shown in Table 3. We attribute this to the much longer side chains and shorter backbones relative to the studies discussed above, and conclude that we can only provide an estimate of the Kuhn length but not a trend with side chain or backbone length.

Using the rigid cylinder model for the radius *R* and length *L*, respectively, we can extract a power-law scaling for the end-to-end distance for both the side chains and backbone:

$$R = l_{SC} \times N_{SC}^{\nu_{SC}}$$

$$L = l_{BB} \times N_B^{\nu_B}$$

where *R* is the end-to-end distance of the side chain, *L* is the end-to-end distance of the backbone, l_{SC} the size of a side chain repeat unit, l_{BB} is the size of a backbone repeat unit,

N_{SC} is the degree of polymerization of the side chains, N_B is the degree of polymerization of the backbone, ν_{SC} is the scaling parameter for the side chain, and ν_B is the scaling exponent for the backbone. Using a size of a PLA and PNB repeat unit of 5.8 and 7.3 Å, derived from calculated bond radii,[52,53] we find a power-law exponent for the side chains of $\nu_{SC} = 0.58$ ($R^2 = 0.986$). For the series of PLA bottlebrushes with $N_{SC} = 30$ and 60, the scaling result predicts a backbone scaling exponent of $\nu_B = 0.74$ ($R^2 = 0.993$) and 0.79 ($R^2 = 0.967$), respectively. Power-law fits for the side chains, and backbone is shown in Figure S10.

Assuming the solvent is a theta-solvent,[54] side chains are only weakly stretched relative to free polymers in solution. This is a smaller exponent than what is predicted through scaling theories[9–12] but consistent with simulations, which have found that the side chains are approximately Gaussian chains.[13] The bottlebrush backbone is more extended than the side chains but retains significant conformational flexibility (a fully extended chain would have an end-to-end distance that scales linearly with N_{BB}). Our measurements indicate significantly greater flexibility for bottlebrushes in solution compared to those in the melt (scaling exponent of 0.9[16]), and our results are in good quantitative agreement with the simulation predictions by Hsu et al. for a bottlebrush polymer in a good solvent, in which they predict $\nu_{SC} = 0.5$ and $\nu_B = 0.7$.

CONCLUSIONS

A series of well-defined bottlebrush polymers with PLA side chains were analyzed by small-angle neutron scattering. Three different models were applied to interpret the neutron scattering data, the empirical Guinier–Porod model, rigid cylinder, and flexible cylinder models. The rigid cylinder model was found to provide the best fit of scattered intensity, and parameters from this model were used in estimates for the end-to-end distances for bottlebrush side chains and backbone. Analysis of the series of bottlebrushes indicates that the side chains are only weakly stretched relative to free Gaussian chains while the backbone is more elongated and has an end-to-end distance scales approximately with $N^{0.77}$. This indicates that bottlebrushes retain significant conformational flexibility in solution.

ACKNOWLEDGMENTS

This work was supported by the NSF Nanosystems Engineering Research Center for Nanotechnology-Enabled Water Treatment (ERC-1449500) and the Welch Foundation for Chemical Research (C-1888). SLP acknowledges support from the National Science Foundation Graduate Fellowship Program (grant # 0940902). The identification of commercial products does not imply endorsement by the National Institute of Standards and Technology nor does it imply that these are the best for the purpose. The SANS part of this work is based upon activities supported in part by the US National Science Foundation under Agreement No. DMR-1508249.

REFERENCES

1 R. Verduzco, X. Li, S. L. Pesek, G. E. Stein, *Chem. Soc. Rev.* **2015**, *44*, 2405–2420.

2 J. Rzayev, *ACS Macro Lett.* **2012**, *1*, 1146–1149.

3 H. Lee, J. Pietrasik, S. S. Sheiko, K. Matyjaszewski, *Prog. Polym. Sci.* **2010**, *35*, 24–44.

4 S. S. Sheiko, B. S. Sumerlin, K. Matyjaszewski, *Prog. Polym. Sci.* **2008**, *33*, 759–785.

5 M. Müllner, A. H. E. Müller, *Polymer* **2016**, *98*, 389–401.

6 S. J. Dalsin, M. A. Hillmyer, F. S. Bates, *ACS Macro Lett.* **2014**, *3*, 423–427.

7 I. Mitra, X. Li, S. L. Pesek, B. Makarenko, B. S. Lokitz, D. Uhrig, J. F. Ankner, R. Verduzco, G. E. Stein, *Macromolecules* **2014**, *47*, 5269–5276.

8 F. C. Sun, A. V. Dobrynin, D. Shirvanyants, H. I. Lee, K. Matyjaszewski, G. J. Rubinstein, M. Rubinstein, S. S. Sheiko, *Phys. Rev. Lett.* **2007**, *99*, 137801.

9 H. P. Hsu, W. Paul, K. Binder, *Macromol. Symp.* **2007**, *252*, 58–67.

10 T. M. Birshtein, O. V. Borisov, Y. B. Zhulina, A. R. Khokhlov, T. A. Yurasova, *Polym. Sci. USSR* **1987**, *29*, 1293–1300.

11 G. H. Fredrickson, *Macromolecules* **1993**, *26*, 2825–2831.

12 N. A. Denesyuk, *Phys. Rev. E* **2003**, *67*, 51803.

13 H. P. Hsu, W. Paul, S. Rathgeber, K. Binder, *Macromolecules* **2010**, *43*, 1592–1601.

14 Y. Xia, A. J. Boydston, R. H. Grubbs, *Angew. Chem. Int. Ed.* **2011**, *50*, 5882–5885.

15 I. I. Potemkin, A. R. Khokhlov, P. Reineker, *Eur. Phys. J. E* **2001**, *4*, 93–101.

16 S. J. Dalsin, T. G. Rions-Maehren, M. D. Beam, F. S. Bates, M. A. Hillmyer, M. W. Matsen, *ACS Nano* **2015**, *9*, 12233–12245.

17 W. Gu, J. Huh, S. W. Hong, B. R. Sveinbjornsson, C. Park, R. H. Grubbs, T. P. Russell, *ACS Nano* **2013**, *7*, 2551–2558.

18 M. Xie, J. Dang, H. Han, W. Wang, J. Liu, X. He, Y. Zhang, *Macromolecules* **2008**, *41*, 9004–9010.

19 W. Gu, J. Huh, S. W. Hong, B. R. Sveinbjornsson, C. Park, R. H. Grubbs, T. P. Russell, *ACS Nano* **2015**, *9*, 7729–7729.

20 S. Rathgeber, T. Pakula, A. Wilk, K. Matyjaszewski, H. Lee, K. L. Beers, *Polymer* **2006**, *47*, 7318–7327.

21 S. Rathgeber, T. Pakula, A. Wilk, K. Matyjaszewski, K. L. Beers, *J. Chem. Phys.* **2005**, *122*, 124904–124913.

22 S. L. Pesek, X. Li, B. Hammouda, K. Hong, R. Verduzco, *Macromolecules* **2013**, *46*, 6998–7005.

23 S. Ahn, J. M. Y. Carrillo, Y. Han, T. H. Kim, D. Uhrig, D. L. Pickel, K. Hong, S. M. Kilbey, B. G. Sumpter, G. S. Smith, C. Do, *ACS Macro Lett.* **2014**, *3*, 862–866.

24 Z. Zhang, J. M. Y. Carrillo, S. Ahn, B. Wu, K. Hong, G. S. Smith, C. Do, *Macromolecules* **2014**, *47*, 5808–5814.

25 G. Cheng, Y. B. Melnichenko, G. D. Wignall, F. Hua, K. Hong, J. W. Mays, *Macromolecules* **2008**, *41*, 9831–9836.

26 S. Bolisetty, C. Airaud, Y. Xu, uuml, A. H. E. Iler, L. Harnau, S. Rosenfeldt, P. Lindner, M. Ballauff, *Phys. Rev. E* **2007**, *75*, 40803.

27 B. Zhang, F. Gröhn, J. S. Pedersen, K. Fischer, M. Schmidt, *Macromolecules* **2006**, *39*, 8440–8450.

28 L. Feuz, P. Strunz, T. Geue, M. Textor, O. Borisov, *Eur. Phys. J. E* **2007**, *23*, 237–245.

29 S. Lecommandoux, F. Chécot, R. Borsali, M. Schappacher, A. Deffieux, A. Brûlet, J. P. Cotton, *Macromolecules* **2002**, *35*, 8878–8881.

30 M. S. Sanford, J. A. Love, R. H. Grubbs, *Organometallics* **2001**, *20*, 5314–5318.

31 Y. Xia, B. D. Olsen, J. A. Kornfield, R. H. Grubbs, *J. Am. Chem. Soc.* **2009**, *131*, 18525–18532.

32 Y. Xia, J. A. Kornfield, R. H. Grubbs, *Macromolecules* **2009**, *42*, 3761–3766.

33 S. R. Kline, *J. Appl. Crystallogr.* **2006**, *39*, 895–900.

34 B. Hammouda, *J. Appl. Crystallogr.* **2010**, *43*, 716–719.

35 J. S. Pedersen, *Curr. Opin. Colloid Interface Sci.* **1999**, *4*, 190–196.

36 G. Fournet, A. Guinier. Small-Angle Scattering of X-Rays; John Wiley and Sons: New York, **1955**.

37 J. S. Pedersen, P. Schurtenberger, *Macromolecules* **1996**, *29*, 7602–7612.

38 J. S. Pedersen, *Adv. Colloid Interface Sci.* **1997**, *70*, 171–210.

39 B. Hammouda, *Polymer* **2009**, *50*, 5293–5297.

40 A. Stradner, H. Sedgwick, F. Cardinaux, W. C. K. Poon, S. U. Egelhaaf, P. Schurtenberger, *Nature* **2004**, *432*, 492–495.

41 P. D. Godfrin, I. E. Zarraga, J. Zarzar, L. Porcar, P. Falus, N. J. Wagner, Y. Liu, *J. Phys. Chem. B* **2016**, *120*, 278–291.

42 E. J. Yearley, P. D. Godfrin, T. Perevozchikova, H. Zhang, P. Falus, L. Porcar, M. Nagao, J. E. Curtis, P. Gawande, R. Taing, I. E. Zarraga, N. J. Wagner, Y. Liu, *Biophys. J.* **2014**, *106*, 1763–1770.

43 J. S. Higgins, H. C. Benoit. Polymers and Neutron Scattering; Clarendon Press: Oxford, **1994**.

44 S. Kawaguchi, K. Ito, *Colloids Surf. Physicochem. Eng. Asp.* **1999**, *153*, 173–178.

45 H. P. Hsu, K. Binder, W. Paul, *Phys. Rev. Lett.* **2009**, *103*, 198301.

46 H. P. Hsu, W. Paul, K. Binder, *Macromol. Theory Simul.* **2011**, *20*, 510–525.

47 K. Terao, Y. Nakamura, T. Norisuye, *Macromolecules* **1999**, *32*, 711–716.

48 K. Terao, Y. Takeo, M. Tazaki, Y. Nakamura, T. Norisuye, *Polym. J. Tokyo Jpn.* **1999**, *31*, 193–198.

49 K. Terao, T. Hokajo, Y. Nakamura, T. Norisuye, *Macromolecules* **1999**, *32*, 3690–3694.

50 T. Hokajo, K. Terao, Y. Nakamura, T. Norisuye, *Polym. J.* **2001**, *33*, 481–485.

51 K. Terao, S. Hayashi, Y. Nakamura, T. Norisuye, *Polym. Bull. 44*, 309–316. **n.d.**,

52 P. Pyykkö, M. Atsumi, *Chem. Eur. J.* **2009**, *15*, 12770–12779.

53 B. Cordero, V. Gómez, A. E. Platero-Prats, M. Revés, J. Echeverría, E. Cremades, F. Barragán, S. Alvarez, *Dalton Trans.* **2008**, 2832–2838.

54 S. Sato, D. Gondo, T. Wada, S. Kanehashi, K. Nagai, *J. Appl. Polym. Sci.* **2013**, *129*, 1607–1617.